Reversible and irreversible voltage manipulation of interfacial magnetic anisotropy in Pt/Co/oxide multilayers

Aymen Fassatoui, Jose Pena Garcia, Laurent Ranno, Jan Vogel, Anne Bernand-Mantel, Hélène Béa, Sergio Pizzini, Stefania Pizzini

Reversible and Irreversible Voltage Manipulation of Interfacial Magnetic Anisotropy in Pt/Co/Oxide Multilayers

Aymen Fassatoui,[1] Jose Peña Garcia,[1] Laurent Ranno,[1] Jan Vogel,[1] Anne Bernard-Mantel,[2] Hélène Béa,[3] Sergio Pizzini,[4] and Stefania Pizzini[1,*]

[1] *University Grenoble Alpes, CNRS, Institut Néel, Grenoble, France*

[2] *Laboratoire de Physique et Chimie des Nano-Objets, Université de Toulouse, Toulouse, France*

[3] *University Grenoble Alpes, CEA, CNRS, Grenoble INP, IRIG-SPINTEC, Grenoble, France*

[4] *Department of Materials Science, University of Milano-Bicocca, Via Cozzi 53 Milano, Italy*

(Received 17 July 2020; revised 19 October 2020; accepted 24 November 2020; published 14 December 2020)

The perpendicular magnetic anisotropy at the Co-oxide interface in Pt/Co/MO_x (MO_x = MgO_x, AlO_x, TbO_x) is modified by an electric field using a 10-nm-thick ZrO_2 as a solid electrolyte. The large voltage-driven modification of the interfacial magnetic anisotropy and the nonvolatility of the effect is explained in terms of the migration of oxygen ions toward or away from the Co/MO_x interface. While the effect is reversible in Pt/Co/AlO_x and Pt/Co/TbO_x, where the Co layer can be oxidized or reduced, in Pt/Co/MgO_x the effect is found to be irreversible. We propose that these differences may be related to the different nature of the ionic conduction within the MO_x layers.

DOI: 10.1103/PhysRevApplied.14.064041

I. INTRODUCTION

The manipulation of the interfacial magnetic anisotropy via an electric field is an active field of research, as it is a promising route toward the realization of low-power spintronic devices [1]. In metallic ferromagnetic (FM) thin films, electric fields have been shown to modify substantially the interface magnetic anisotropy energy through the modification of the electron density of states at the Fermi energy, despite their short penetration depth, which is limited by Coulomb screening [2–5]. The perpendicular magnetic anisotropy (PMA) at a FM-oxide interface can be as large as that found at a heavy-metal–Co interface [6]. *Ab initio* calculations suggest that this anisotropy results from the hybridization of the oxygen and transition-metal electronic orbitals across the interface [7]. Several experimental studies of Pt/Co/MO_x trilayers (M = Al, Mg, Ta, etc.) have shown that the PMA amplitude is related to the degree of oxidation of the Co layer. The interfacial anisotropy constant (K_s^{ox}) at the Co/MO_x interface has a characteristic bell-like shape, with a maximum for the optimal oxidation conditions (see the sketch in Fig. 1), obtained when the oxygen atoms reach the Co/M interface, so that Co—O bonds prevail over Co—M bonds [8–11]. It is then not surprising that the largest effects of an electric field on the PMA ($\Delta K_s/E = \beta > 1000$ fJ/Vm) have been obtained by triggering the migration of oxygen ions toward or away from the FM-oxide interface [12–14]. This magneto-ionic effect, obtained in most cases using Gd_2O_3 as dielectric oxide layer, leads to a nonvolatile modification of the interfacial PMA, as opposed to the volatile effect obtained by electron accumulation or depletion. Also, the time scales associated with the electric-field-induced displacement of electrons or ions are different.

In the present work, we describe the effect of an electric field on the interfacial PMA in a series of Pt/Co/MO_x (M = Mg, Al, Tb) trilayers. Beyond their interest because of their tunable PMA, these noncentrosymmetric systems have largely been studied because they can host chiral magnetic textures such as chiral domain walls (DWs) and magnetic skyrmions, due to the presence of the interfacial Dzyaloshinskii-Moriya interaction (DMI). By tuning the PMA [15–21] and/or the DMI at the FM-oxide interface [22–24], it has been shown that the electric field can modify the stability and the field- and current-driven dynamics of such magnetic textures.

Through the use of 10-nm-thick ZrO_2 as a dielectric layer deposited on top of the Pt/Co/MO_x stack, we demonstrate that the effect of the electric field on the PMA is large ($\beta > 1200$ fJ/Vm at room temperature) and nonvolatile. The tuning of the magnetic anisotropy allows us to stabilize a variety of magnetic configurations within the Co layers and to modify the details of the magnetic reversal mechanisms. The nonvolatility of the magnetic structures obtained after the removal of the gate voltage, the characteristic time evolution of the electric field effect, and its large efficiency can be understood by considering the ZrO_2 as a solid electrolyte, working as an oxygen-ion

*stefania.pizzini@neel.cnrs.fr

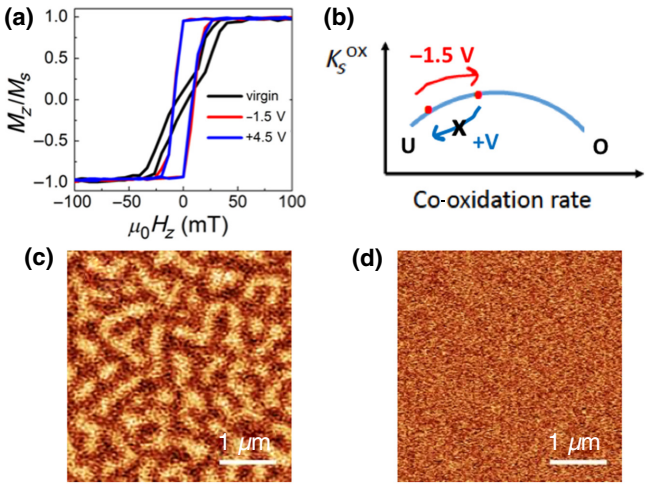

FIG. 1. The nonvolatile and irreversible effect of the electric field in the Pt/Co/MgO_x magnetic stack. (a) Kerr hysteresis loops measured for a Pt/Co/MgO_x sample below the top Pt electrode, in the virgin state ($V_g = 0$), after the application of $V_g = -1.5$ V for 30 s, leading to an increase of the interfacial PMA, and subsequently after the application of $V_g = +4.5$ V for 120 s, showing that the square loop, i.e., the larger PMA, is maintained. (b) A sketch representing the variation of the interfacial anisotropy K_s^{ox} versus the Co layer oxidation rate [8–11] and the effect of the gate voltage; at the extremities of the K_s^{ox} curve, "O" denotes overoxidized Co and "U" underoxidized Co with respect to the optimal oxidation giving maximum PMA. (c) A MFM image showing the labyrinthine domain configuration in the virgin state. (d) A MFM image after the application of $V_g = -1.5$ V for 30 s. During the image scans, neither a voltage nor an out-of-plane magnetic field is applied. The dark and light contrasts correspond to down and up magnetization.

conductor. While the effect is reversible in Pt/Co/AlO_x and Pt/Co/TbO_x, where the Co layer can be oxidized or reduced, in Pt/Co/MgO_x the effect is found to be irreversible. Once the PMA has increased by increasing the Co oxidation, the reverse process does not occur by polarization inversion. We propose that this different behavior may be related to the specific nature of the ionic conduction within the different MO_x layers.

II. METHODS: FILM DEPOSITION AND PATTERNING

Pt(3)/Co(1)/Mg(0.7), Pt(3)/Co(1)/Al(1), and Pt(3)/Co(1.1-1.2)/Tb(0.6) trilayers (thicknesses in nanometers) are deposited by magnetron sputtering on Si/SiO_2 wafers. The Mg and Tb layers are oxidized in an oxygen atmosphere, while the Al layer is oxidized in an oxygen plasma at room temperature. The trilayers are patterned into 1–50-μm-wide strips by electron-beam lithography and ion-beam milling. A 10-nm-thick ZrO_2 dielectric layer is then deposited on top of the samples by atomic layer deposition (ALD). Finally, following a second lithography step, a 6-nm-thick Pt layer is evaporated on top of the strips, leading to local gates. In the three magnetic stacks, the Co layer is underoxidized relative to the optimal oxidation corresponding to the maximum PMA (see [8–11] and the sketches in Figs. 1–3). For more details on the fabrication methods, see the Supplemental Material [25].

The electric field is applied across the Pt electrodes, with the top one being grounded. The bias voltage is defined as $V_g = V_{top} - V_{bottom}$, in order to keep the usual sign convention. Unless specified, the bias voltage is applied with the sample being at room temperature. The magnetic configuration of the Co layer below the electrode regions is observed using magnetic force microscopy (MFM) for Pt/Co/MgO_x and Pt/Co/TbO_x and using polar magneto-optical Kerr microscopy for Pt/Co/AlO_x. The hysteresis loops are measured using magneto-optical Kerr effect (MOKE) magnetometry. Note that the hysteresis loops and the magnetic images are always measured with $V_g = 0$ V, either in the as-prepared (virgin) state or after the application of the electric field, once V_g is removed and the new magnetic state is imprinted in the Co layer.

III. NONVOLATILE AND IRREVERSIBLE MANIPULATION OF INTERFACIAL PMA IN Pt/Co/MgO_x

The hysteresis loop measured for the Pt/Co/MgO_x trilayer exhibits a butterflylike shape with low remanence, indicating thermally activated formation of magnetic domains [Fig. 1(a)]. The MFM image confirms the presence of labyrinthine domains with out-of-plane magnetization, with an average width of $\simeq 120$ nm [Fig. 1(c)].

The formation of labyrinthine domains is the consequence of the balance between the demagnetizing energy and the domain-wall energy in a perpendicularly magnetized system. This magnetic configuration can be observed in the vicinity of the reorientation transition from in-plane (IP) to out-of-plane (OOP) magnetization, when the effective magnetic anisotropy K_{eff} is close to zero and changes sign:

$$K_{eff} = \frac{K_s}{t_{Co}} - \frac{1}{2}\mu_0 M_s^2 = \frac{K_s^{ox} + K_s^{Pt}}{t_{Co}} - \frac{1}{2}\mu_0 M_s^2 \simeq 0, \quad (1)$$

where K_s is the interfacial anisotropy constant, with K_s^{Pt} and K_s^{ox} being the contributions from the Co/Pt and Co/MO_x interfaces, and M_s is the spontaneous magnetization.

The labyrinthine domain width L in the case of ultrathin ferromagnetic layers is given by [26,27]

$$L = Ct \exp \frac{\pi L_0}{t}, \quad (2)$$

where $L_0 = \sigma/\mu_0 M_s^2$ is the characteristic dipolar length; σ is the domain-wall energy, t is the ferromagnetic film thickness, and C is a numerical constant of the order of 1. In the noncentrosymmetric stacks studied in this work, the domain walls have a chiral Néel structure [28,29] and their energy is given by $\sigma = (4\sqrt{AK_{\text{eff}}} - \pi|D|)$, where A is the exchange stiffness and D is the strength of the DMI. The observed labyrinthine structure can be reproduced by micromagnetic simulations using experimentally relevant magnetic parameters (see the Supplemental Material [25]; see also Refs. [29–31]).

After the application of a bias voltage $V_g = -1.5$ V for 30 s, the stripe domains disappear and a magnetic state with 100% remanence at zero field is obtained, as shown by the square hysteresis loop [Fig. 1(a)] and the MFM image [Fig. 1(d)]. This indicates that the negative voltage drives the increase of the interfacial anisotropy K_s^{ox} which, as sketched in [Fig. 1(b)], can be associated to the increase of the Co oxidation. The same magnetic state is maintained for several weeks after the removal of the electric field, i.e., the change of magnetic properties driven by the electric field can be defined as nonvolatile. Figure 1(a) shows that after the application of a reverse voltage $V_g = +4.5$ V for 2 min, the hysteresis loop stays unchanged. The application of a much larger bias voltage ($V_g = +12$ V) for several minutes does not change the shape of the hysteresis loop, which remains square: the electric field effect on the magnetization appears to be irreversible.

IV. NONVOLATILE AND REVERSIBLE MANIPULATION OF INTERFACIAL PMA IN Pt/Co/AlO$_x$

In the virgin state, the Co layer in Pt/Co/AlO$_x$ presents an out-of-plane magnetization, with a square hysteresis loop showing a saturated magnetic state at remanence [Fig. 2(a)]. Following the application of positive voltages ranging from +1.5 V to +2.5 V for 30 s, the hysteresis loops

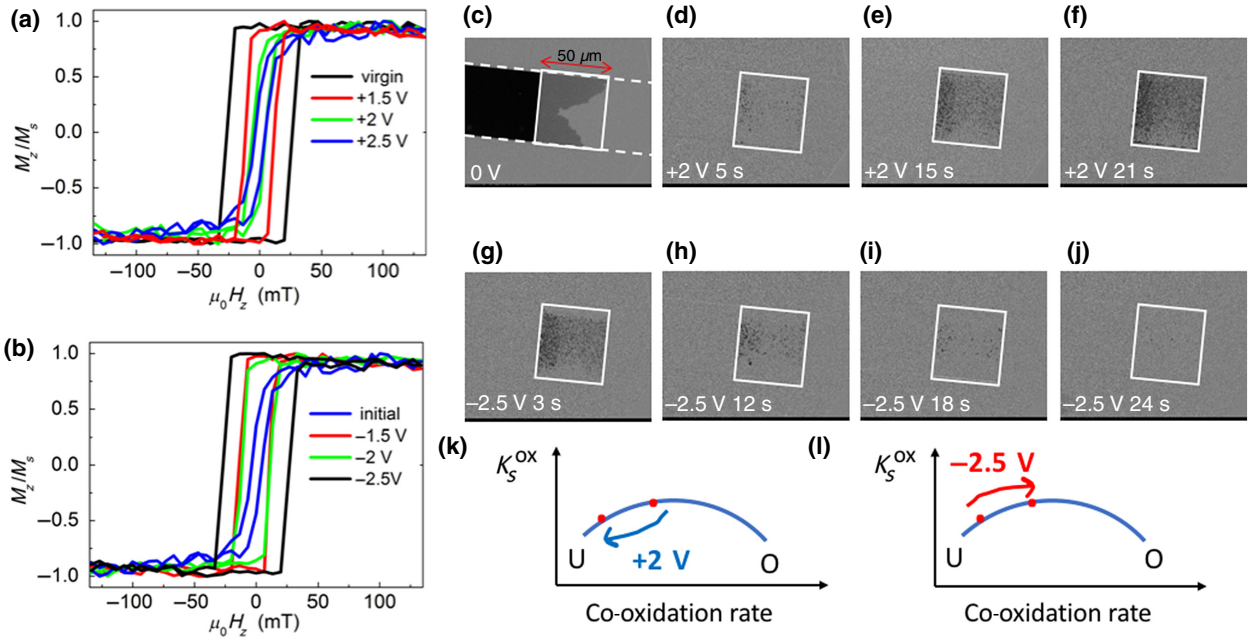

FIG. 2. The nonvolatile and reversible effect of the electric field in the Pt/Co/AlO$_x$ magnetic stack. (a) Hysteresis loops measured below the top Pt electrode in the virgin state and after the application of positive bias voltages $V_g = +1.5$ V, +2 V, and +2.5 V for 30 s, leading to the decrease of coercivity associated with the decrease of the interfacial PMA. (b) Hysteresis loops measured after the application of negative bias voltages $V_g = -1.5$ V, −2 V, and −2.5 V for 30 s, leading to the increase of the anisotropy; the initial state of this series of loops is the one obtained after the application of $V_g = +2.5$ V for 30 s in (a). (c) A differential Kerr image showing the reversal by domain-wall propagation in the virgin state. (d)–(j) Differential Kerr images showing the effect of (d)–(f) positive and, subsequently, (g)–(j) negative bias voltages on the nucleation rate of the reversed domains. Each hysteresis loop and each image is taken *after* the application of the electric field, i.e., with $V_g = 0$ V; the nucleation of the reversed domains in (d)–(j) is obtained by applying a field pulse $B_z = -26$ mT for 20 ms after saturation with $+B_z$; for (c), several pulses are applied to bring the reversed domains within the electrode region. The white squares indicate the location of the top electrode within the magnetic stripes [dotted lines in (c)]. (k)–(l) Sketches representing the variation of the interfacial anisotropy constant K_s^{ox} versus the Co-layer oxidation rate and the effect of the (k) positive and (l) negative gate voltage. "O" denotes overoxidized Co and "U" underoxidized Co with respect to the optimal oxidation giving maximum PMA.

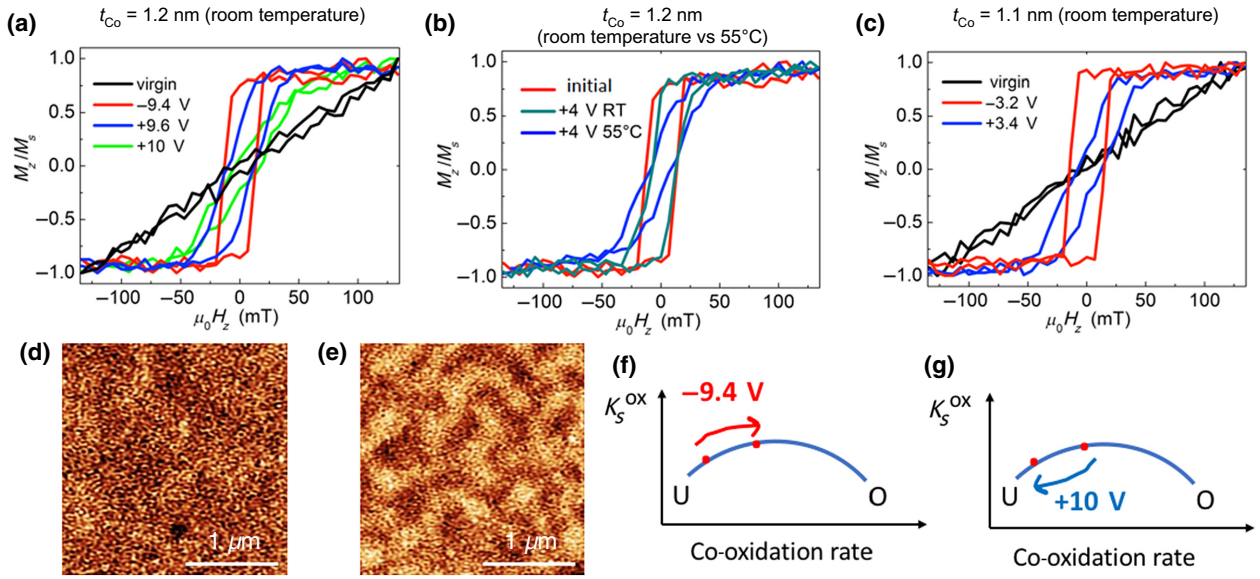

FIG. 3. The nonvolatile and reversible effect of the electric field in the Pt/Co/TbO_x magnetic stack. (a) Hysteresis loops measured in the virgin state (IP magnetization), after the application of $V_g = -9.4$ V for 30 s (increasing the PMA) and, subsequently, $V_g = +9.6$ V and $+10$ V for 30 s (decreasing the PMA) at room temperature for a sample with $t_{Co} = 1.2$ nm. (b) Hysteresis loops measured in the initial state [square loop obtained after $V_g = -9.4$ V for 30 s in (a)] and after the application of $V_g = +4$ V for 30 s with the sample at room temperature and at 55 °C. (c) Hysteresis loops measured in the virgin state (IP magnetization), after the application of $V_g = -3.2$ V for 30 s (increasing the PMA) and, subsequently, $V_g = +3.4$ V (decreasing the PMA) for 30 s at room temperature for a stack with $t_{Co} = 1.1$ nm. (d) A MFM image obtained after the application of $V_g = -9.4$ V for 30 s, starting from the virgin state, leading to saturated OOP magnetization. (e) A MFM image obtained after the consequent application of $V_g = +10$ V for 30 s, leading to labyrinthine domains. The dark and light contrasts correspond to down and up magnetization. (f),(g) Sketches representing the variation of the interfacial anisotropy constant K_s^{ox} versus the Co layer oxidation rate and the effect of the (f) negative and (g) positive gate voltage. "O" denotes overoxidized Co and "U" underoxidized Co with respect to the optimal oxidation giving maximum PMA.

(always measured after the voltage is removed, $V_g = 0$ V) illustrate a progressive decrease of the coercive field, indicating a decrease of the interfacial PMA. As sketched in Fig. 2(k), this points to a decrease of the oxidation of the Co layer. When the reverse voltage is applied [from -1.5 V to -2.5 V for 30 s, Fig. 2(b)], the opposite process occurs: the gradual widening of the hysteresis loops suggests the increase of PMA, related to the increase of the Co oxidation [Fig. 2(l)] up to the recovery of a hysteresis loop with a coercive field similar to the initial one. The effect is therefore nonvolatile and reversible.

The modification of the interfacial PMA can also be deduced from the voltage-induced variation of the magnetization-reversal process, as illustrated by the differential MOKE microscopy images shown in Figs. 2(c)–2(j). In the virgin state [Fig. 2(c)], the magnetization reversal occurs via the expansion of a few large domains, as expected in magnetic layers with sufficiently large anisotropy. The magnetic configurations shown in Figs. 2(d)–2(j) are obtained as follows: after the application of a bias voltage $V_g = +2$ V or $V_g = -2.5$ V for a duration t between 2 and 24 s, the samples are magnetically saturated in the OOP direction with a field $+B_z$. A 20-ms pulse $B_z = -26$ mT is then applied to reverse the magnetization. The images show that after the application of a positive voltage $V_g = +2$ V that decreases the interfacial anisotropy K_s^{ox}, the magnetization-reversal mechanism changes and is dominated by the nucleation of a large density of domains, the domain density increasing as the application time of the voltage increases. This may be explained within the droplet model [32], which predicts that the height of the energy barrier for nucleation is $\Delta E_n = \pi\sigma^2 t/2M_s\mu_0 H$, where σ is the domain-wall energy, t is the film thickness, and $\mu_0 H$ is the applied magnetic field [33]. Since σ decreases when the effective anisotropy decreases, nucleation may dominate the magnetization reversal in disordered samples with low average magnetic anisotropy, where the large distribution of anisotropy fields (i.e., of local defects) may hinder the domain-wall movement. As the application time of the positive voltage increases, the density of the reversed domains increases, indicating the progressive decrease of the PMA [34,35] associated with the progressive migration of oxygen ions away from the Co interface. Note that no nucleation event is observed outside the electrode region, where the PMA remains large and the applied field pulse is not sufficient to overcome the nucleation barriers. When

the negative bias voltage is applied for increasing times, starting from the configuration with the lowest PMA [Fig. 2(f)], the density of reverse domains gradually decreases, in agreement with the increase of the PMA suggested by the increase of coercivity in the hysteresis loops.

V. NONVOLATILE AND REVERSIBLE MANIPULATION OF INTERFACIAL PMA IN Pt/Co/TbO$_x$

Figure 3(a) shows the polar MOKE hysteresis loops acquired for Pt/Co/TbO$_x$ in a sample with $t_{Co} = 1.2$ nm. In the virgin state, the loop is tilted, as expected for in-plane magnetization. After the application of a bias voltage $V_g = -9.4$ V for 30 s, the hysteresis loop becomes square, indicating an increase of the PMA and the switch to a remanent saturated out-of-plane magnetization. By applying an opposite voltage ($V_g = +9.6$ V for 30 s) the anisotropy decreases, giving rise to a loop reminiscent of the presence of labyrinthine domains in a zero field. When $V_g = +10$ V is applied for 30 s, the anisotropy can be further decreased, leading to in-plane magnetization orientation as in the initial state.

The voltage-induced modification of the magnetization state is nonvolatile and, as for Pt/Co/AlO$_x$, the interfacial magnetic anisotropy can be tuned in a reversible way.

The MFM images shown in Figs. 3(d)–3(e) confirm the modification of the magnetic configuration by the electric field. The image with homogenous contrast observed after the application of $V_g = -9.4$ V for 30 s [Fig. 3(d)] confirms the saturated magnetic state at remanence already indicated by the hysteresis loop. After the application of $V_g = +10$ V for 30 s [the butterflylike hysteresis loop in Fig. 3(a)], the presence of a demagnetized state with labyrinthine domains [Fig. 3(e)] is in agreement with the decrease of the interfacial PMA.

If the sample temperature is increased to 55 °C during the application of the electric field, the voltage necessary to switch from a square loop (OOP magnetization) to a butterfly loop (labyrinthine domains) is of the order of +4 V for 30 s [Fig. 3(b)] instead of +9.6 V for 30 s at room temperature [Fig. 3(a)]. The kinetics of the oxidation process is therefore enhanced by the temperature.

When the bias voltage is applied to a sample with a thinner Co layer ($t_{Co} = 1.1$ nm), the voltage necessary to switch the magnetization from in-plane to out-of-plane at room temperature is reduced to $V_g = -3.2$ V for 30 s and a positive voltage $V_g = +3.4$ V for 30 s is sufficient to obtain a butterfly loop [Fig. 3(c)].

VI. DISCUSSION: MICROSCOPIC MECHANISMS

Our results show that the interfacial magnetic anisotropy at the Co/MO$_x$ interface in Pt/Co/MO$_x$ trilayers can be strongly modified by a gate voltage, using a 10-nm-thick ZrO_2 dielectric layer deposited by ALD on top of the magnetic stack. A negative (positive) gate voltage leads to an increase (decrease) of the PMA, which we correlate with an increase (decrease) of the oxidation of the initially underoxidized Co layers. The efficiency of the effect is measured to be > 1200 fJ/Vm for Pt/Co/AlO$_x$ at room temperature (see the Supplemental Material [25]) and similar values can be expected for Pt/Co/TbO$_x$ and Pt/Co/MgO$_x$. These values are comparable to the highest reported in the literature in cases where the gate voltage applied at high temperature has triggered oxygen-ion migration [12,13] or where the sample has been hydrated, giving rise to conduction dominated by hydrogen ions [36,37]. In all these cases, Gd_2O_3 has been used as an ion-conductor layer.

In Pt/Co/AlO$_x$ and Pt/Co/TbO$_x$, the nonvolatility and the reversibility of the effect, the large voltage-induced modification of the interfacial PMA at the Co-oxide interface, and its dependence on the strength or the duration of the applied voltage suggest that the driving mechanism might be the migration of oxygen ions across the ZrO_2 dielectric layer.

Negative (positive) gate voltages, driving O^{2-} ions toward (away) from the Co layer, would lead to an increase (decrease) of the Co oxidation. Since the Co layers are initially underoxidized with respect to the optimal oxidation, this should give rise to an increase (decrease) of the interfacial anisotropy, as observed experimentally [see the sketches in Figs. 1(b), 2(k), 2(l), 3(f), and 3(g)]. These features therefore confirm, as found by previous works [8–10,20], that the modification of the observed PMA is associated with the variation of the oxidation of the Co/MO$_x$ interface.

The interpretation of the effect in terms of oxygen-ion migration can also explain the results shown in Figs. 3(b) and 3(c) for Pt/Co/TbO$_x$. When the sample is heated during the application of the electric field, the drift velocity of the oxygen ions is expected to increase [38], so that the same Co oxidation state (i.e., the same change of PMA) can be reached over the same time period with a weaker electric field. Similarly, we observe that the voltage needed to switch the magnetization from in-plane to out-of-plane decreases as the Co thickness decreases [Figs. 3(a) and 3(c)]. This result can be related to the $1/t_{Co}$ dependence of the interfacial magnetic anisotropy energy [Eq. (1)]: for an underoxidized Co layer with constant K_s^{ox} (constant oxidation) and variable thickness, the increase of K_s^{ox}, and therefore of oxidation, necessary to reorient the magnetization in the OOP direction is smaller for the thinner layer. This can then be realized, for the same bias duration, with a lower electric field.

In the case of Pt/Co/MgO$_x$, the irreversibility of the electric field effect suggests that oxygen-ion migration alone cannot account for the overall process features and that some irreversible step should occur, causing the permanence of the oxidation of Co at the Co/MgO

interface, even after the application of a strong reverse polarization.

In this work, the PMA is manipulated while keeping the Co layer underoxidized. Of course, we expect that the PMA will decrease, as a result of the overoxidation of the Co layer, if the negative bias voltage is increased or applied for longer times after reaching the maximum anisotropy.

The reversible or irreversible manipulation of the PMA in the systems described in this work can be discussed by considering the Pt/Co/MO_x/ZrO_2/Pt (M = Mg, Al, Tb) system as a solid-state nanometric galvanic cell, where the 10-nm-thick ZrO_2 layer works as a solid electrolyte with pure O^{2-} conductivity and where the Al, Mg or Tb ultrathin oxides also work as solid electrolytes with pure ionic conductivity or mixed ionic and electronic conductivity.

The oxidation of the Mg, Al, and Tb films deposited above the Co layer is driven by the large values of the Gibbs free energies of formation of the oxides [39]. For Mg and Al, we expect the formation of stoichiometric (or slightly understoichiometric) MgO and Al_2O_3 films, while in the case of Tb, the formation of a mixed valence (Tb^{3+} and Tb^{4+}) nonstoichiometric oxide TbO_{2-x} can be foreseen.

According to the results of Subba Rao *et al.* [40], which relate to terbium sesquioxide prepared at high temperature, and to recent results of Miran *et al.* [41] on the presence of surface oxygen vacancies in TbO_2, this oxide, like all reduced oxides of the ceria family [42], should present, in the bulk phase, predominant electronic conductivity, with significant ionic conductivity associated with oxygen vacancies. The presence of more than one phase in nanocrystalline or amorphous terbium oxide [43] makes it extremely difficult to quantitatively predict its behavior, although its mixed ionic-electronic conductivity may be safely foreseen, with O^{2-} as the ionic carrier.

The ionic transport properties of MgO and Al_2O_3 are, instead, fully defined, since nanosized MgO exhibits Mg^{2+} ionic conductivity [44] and Al_2O_3 exhibits ionic conductivity due to oxygen ions [45], although we cannot exclude a small contribution of electronic conductivity for the nonstoichiometric oxides.

The reversibility associated with the use of Al_2O_3 as a solid-state electrolyte in the cell Pt/Co/Al_2O_3/ZrO_2/Pt can, therefore, be easily understood if we assume that the top Pt electrode behaves as a sink for atmospheric oxygen and works as a reversible oxygen electrode,

$$\mathrm{O(Pt)} + 2e \leftrightarrow \mathrm{O}^{2-}, \tag{3}$$

at room temperature, with the formation of oxygen ions O^{2-}. In the case of forward polarization (negative V_g), these can be moved into the ZrO_2 layer, which enables oxygen-ion transfer, and then to the Al_2O_3 layer to the Al_2O_3/Co interface, where each incoming oxygen ion can form hybrid bonds with a Co surface atom:

$$\mathrm{Co} + \mathrm{O}^{2-} \leftrightarrow O_{\mathrm{Co}}^{\mathrm{surf}} + 2e, \tag{4}$$

where O_{Co}^{surf} is an oxygen bonded at the Co top surface of the Co layer.

If the process in Eq. (4) is also reversible, under reverse polarization (positive V_g) oxygen can be transferred backward to the top Pt electrode and the surface of Co can be deoxidized, in agreement with the experimental results.

For TbO_{2-x} in the Pt/Co/TbO_{2-x}/ZrO_2/Pt cell, we may, again, assume the occurrence of the same reversible electrode reactions and transfer processes of O^{2-} ions, but in parallel with the direct Co oxidation reaction [Eq. (4)], a parasitic reaction involving the nonstoichiometric Tb oxide may occur, with the TbO_{2-x} layer working as a parasitic oxygen electrode, the behavior of which can be formally described by the following reversible reaction:

$$\mathrm{TbO}_{2-x} + 2ye \leftrightarrow \mathrm{TbO}_{2-z} + y\mathrm{O}^{2-}, \tag{5}$$

where $z = x - y$, which leads to a minute change of the stoichiometry of the Tb oxide. Therefore, also with the use of TbO_x, we expect a full reversibility of the entire process but with a Co oxidation efficiency lower than in the case of the use of Al_2O_3 as electrolyte, due to the parasitic process.

The same overall oxygen transport features cannot be expected to occur in the case of a MgO_x layer, due to its Mg^{2+} ionic conductivity [44], but the nonvolatile and irreversible oxidation of the Co surface under forward bias may still be understood. While we expect the reaction in Eq. (3) to occur at the reversible Pt electrode, with the formation of oxygen ions O^{2-}, and their further transfer in the ZrO_2 layer down to the ZrO_2/MgO_x interface, the oxygen transport is blocked in the MgO_x layer.

When the Pt electrode is polarized under forward bias ($-V_g$), the process occurring at the Co/MgO_x interface can be described by the following electrode reaction:

$$\mathrm{Co} + x\mathrm{MgO} \rightarrow xO_{\mathrm{Co}}^{\mathrm{surf}} + x\mathrm{Mg}^{2+} + 2xe, \tag{6}$$

which induces a surface oxidation of Co via the partial electroreduction of the MgO_x phase. If we further assume that an ionic carrier interchange occurs at the ZrO_2/MgO_x interface, where O^{2-} ions injected by the Pt(O) electrode interact with the incoming Mg^{2+} ions arriving from the Co/MgO_x interface, with the irreversible formation of a MgO phase,

$$\mathrm{O}^{2-} + \mathrm{Mg}^{2+} \rightarrow \mathrm{MgO}, \tag{7}$$

this then enables an ionic current to flow across the entire cell.

The reaction in Eq. (6) could occur as a reversible process, although under severe kinetic hindrances. However, the carrier interchange at the ZrO_2/MgO_x interface under reverse bias does not occur, since the MgO_x phase at the ZrO_2/MgO_x interface cannot behave as a source of oxygen ions and thus cannot enable an ionic current to flow across the entire cell. Therefore, we cannot expect that under reverse polarization the system can restore its primitive configuration, in good agreement with the experimental results.

The specificity of the $Pt/Co/MgO_x/ZrO_2/Pt$ system in which we have found an irreversible effect of the electric field may therefore be related to the different nature of the ionic conduction within the MgO_x oxide layer, where it is due to Mg^{2+} cations.

It should be noted that in the three systems, the voltage-driven tuning of the oxidation of the Co/MO_x interface is expected to give rise to a variation of the DMI present at that interface [22,46]). According to our previous work [46], we expect that the variation of the DMI strength will be proportional to the variation of the PMA and to be around +0.2 pJ/m (i.e., around 15% of the total DMI) when varying the Co interface from underoxidized and optimally oxidized. Although this variation of the DMI is expected to have an influence on the domain dynamics and the barrier for nucleation of reversed domains, its impact is expected to be negligible with respect to that associated with the change of K_s^{ox}.

VII. CONCLUSIONS

In conclusion, the perpendicular magnetic anisotropy at the Co/MO_x interface in $Pt/Co/MO_x$ trilayers is modified by an electric field using a ZrO_2 layer working as a solid electrolyte. The tuning of the magnetic anisotropy allows us to stabilize a variety of magnetic configurations within the Co layers and to modify the details of the magnetic reversal mechanisms. The large efficiency and the nonvolatility of the effect, together with its characteristic time evolution, can be explained in terms of the migration of oxygen ions toward or away from the Co/MO_x interface. While the effect is reversible in $Pt/Co/AlO_x$ and $Pt/Co/TbO_x$, where the Co layer can be oxidized or reduced, in $Pt/Co/MgO_x$ the effect is found to be irreversible. We attribute these differences to the different nature of the ionic conduction within the MO_x layer. The large voltage control of magnetic anisotropy ($\beta > 1200$ fJ/Vm in $Pt/Co/AlO_x$) realized with the sample maintained at room temperature is comparable to that reported in the literature using much higher temperatures [12,13] or in hydrated samples [36,37]. This encourages us to continue exploring the use of ZrO_2 with the prospect of finding routes toward a faster manipulation of interfacial anisotropy.

ACKNOWLEDGMENTS

We acknowledge the support of the Agence Nationale de la Recherche (Projects No. ANR-17-CE24-0025 (TOPSKY), No. ANR-16-CE24-0018 (ELECSPIN), and No. ANR-19-CE24-0019 ADMIS) and of the DARPA TEE program through Grant No. MIPR HR0011831554. J.P.G. acknowledges the European Union's Horizon 2020 research and innovation program under Marie Sklodowska-Curie Grant Agreement No. 754303 and the support from the Laboratoire d'Excellence LANEF in Grenoble (Grant No. ANR-10-LABX-0051). B. Fernandez, Ph. David, D. Lepoittevin, and E. Mossang are acknowledged for their technical help. We thank Olivier Fruchart for introducing A.F. to the world of MFM experiments.

[1] T. Nozaki, T. Yamamoto, S. Miwa, M. Tsujikawa, M. Shirai, S. Yuasa, and Y. Suzuki, Recent progress in the voltage-controlled magnetic anisotropy effect and the challenges faced in developing voltage-torque MRAM, Micromachines **10**, 327 (2019).

[2] M. Weisheit, S. Fähler, A. Marty, Y. Souche, C. Poinsignon, and D. Givord, Electric field-induced modification of magnetism in thin-film ferromagnets, Science **315**, 349 (2007).

[3] T. Maruyama, Y. Shiota, T. Nozaki, K. Ohta, N. Toda, M. Mizuguchi, A. A. Tulapurkar, T. Shinjo, M. Shiraishi, and S. Mizukami, Large voltage-induced magnetic anisotropy change in a few atomic layers of iron, Nat. Nanotech. **4**, 158 (2009).

[4] Y. Shiota, T. Nozaki, F. Bonell, S. Murakami, T. Shinjo, and Y. Suzuki, Induction of coherent magnetization switching in a few atomic layers of FeCo using voltage pulses, Nat. Mater. **11**, 39 (2011).

[5] F. Matsukura, Y. Tokura, and H. Ohno, Control of magnetism by electric fields, Nat. Nanotech. **10**, 209 (2015).

[6] S. Monso, B. Rodmacq, S. Auffret, G. Casali, F. Fettar, B. Gilles, B. Dieny, and P. Boyer, Crossover from in-plane to perpendicular anisotropy in $Pt/CoFe/AlO_x$ sandwiches as a function of Al oxidation: A very accurate control of the oxidation of tunnel barriers, Appl. Phys. Lett. **80**, 4157 (2002).

[7] H. X. Yang, M. Chshiev, B. Dieny, J. H. Lee, A. Manchon, and K. H. Shin, First-principles investigation of the very large perpendicular magnetic anisotropy at Fe/MgO and Co/MgO interfaces, Phys. Rev. B **84**, 054401 (2011).

[8] A. Manchon, C. Ducruet, L. Lombard, S. Auffret, B. Rodmacq, B. Dieny, S. Pizzini, J. Vogel, V. Uhlíř, M. Hochstrasser, and G. Panaccione, Analysis of induced anisotropy crossover in $Pt/Co/MO_x$ trilayers, J. Appl. Phys. **104**, 043914 (2008).

[9] A. Manchon, S. Pizzini, J. Vogel, V. Uhlíř, L. Lombard, C. Ducruet, S. Auffret, B. Rodmacq, B. Dieny, M. Hochstrasser, and G. Panaccione, X-ray analysis of oxygen-induced perpendicular magnetic anisotropy in

Pt/Co/AlO_x trilayers, J. Magn. Magn. Mater. **320**, 1889 (2008).

[10] A. Manchon, S. Pizzini, J. Vogel, V. Uhlíř, L. Lombard, C. Ducruet, S. Auffret, B. Rodmacq, B. Dieny, M. Hochstrasser, and G. Panaccione, X-ray analysis of the magnetic influence of oxygen in Pt/Co/AlO_x trilayers, J. Appl. Phys. **103**, 07A912 (2008).

[11] B. Dieny and M. Chshiev, Perpendicular magnetic anisotropy at transition metal/oxide interfaces and applications, Rev. Mod. Phys. **89**, 025008 (2017).

[12] C. Bi, Y. Liu, T. Newhouse-Illige, M. Xu, M. Rosales, J. W. Freeland, O. Mryasov, S. Zhang, S. G. E. Velthuis, and W. G. Wang, Reversible Control of Co Magnetism by Voltage Induced Oxidation, Phys. Rev. Lett. **113**, 267202 (2014).

[13] U. Bauer, Y. Lide, J. T. Aik, P. Agrawal, S. Emori, H. L. Tuller, S. van Dijken, and G. S. D. Beach, Magneto-ionic control of interfacial magnetism, Nat. Mater. **14**, 174 (2015).

[14] X. Zhou, Y. Yan, M. Jiang, B. Cui, F. Pan, and C. Song, Role of oxygen ion migration in the electrical control of magnetism in Pt/Co/Ni/HfO_2 films, J. Physical Chem. C **120**, 1633 (2016).

[15] U. Bauer, S. Emori, and G. S. D. Beach, Electric field control of domain wall propagation in Pt/Co/GdOx films, Appl. Phys. Lett. **100**, 192408 (2012).

[16] U. Bauer, S. Emori, and G. S. D. Beach, Voltage-controlled domain wall traps in ferromagnetic nanowires, Nat. Nanotech. **8**, 411 (2013).

[17] D. Chiba, M. Kawaguchi, S. Fukami, N. Ishiwata, K. Shimamura, K. Kobayashi, and T. Ono, Electric-field control of magnetic domain-wall velocity in ultrathin cobalt with perpendicular magnetization, Nat. Commun. **3**, 888 (2012).

[18] A. J. Schellekens, A. van den Brink, J. H. Franken, H. J. M. Swagten, and B. Koopmans, Electric-field control of domain wall motion in perpendicularly magnetized materials, Nat. Commun. **3**, 847 (2012).

[19] W. Lin, N. Vernier, G. Agnus, K. Garcia, B. Ocker, W. Zhao, E. E. Fullerton, and D. Ravelosona, Universal domain wall dynamics under electric field in Ta/CoFeB/MgO devices with perpendicular anisotropy, Nat. Commun. **7**, 13532 (2016).

[20] A. Bernand-Mantel, L. Herrera-Diez, L. Ranno, S. Pizzini, J. Vogel, D. Givord, S. Auffret, O. Boulle, I. M. Miron, and G. Gaudin, Electric-field control of domain wall nucleation and pinning in a metallic ferromagnet, Appl. Phys. Lett. **102**, 122406 (2013).

[21] M. Schott, A. Bernand-Mantel, L. Ranno, S. Pizzini, J. Vogel, H. Béa, C. Baraduc, S. Auffret, G. Gaudin, and D. Givord, The skyrmion switch: Turning magnetic skyrmion bubbles on and off with an electric field, Nano Lett. **17**, 3006 (2016).

[22] T. Srivastava, M. Schott, R. Juge, V. Křižáková, M. Belmeguenai, Y. Roussigné, A. Bernand-Mantel, L. Ranno, S. Pizzini, S. Chérif, A. Stashkevich, S. Auffret, O. Boulle, G. Gaudin, M. Chshiev, C. Baraduc, and H. Béa, Large voltage tuning of Dzyaloshinskii-Moriya interaction: A route towards dynamic control of skyrmion chirality, Nano Lett. **18**, 4871 (2018).

[23] L. Herrera Diez *et al.*, Nonvolatile Ionic Modification of the Dzyaloshinskii-Moriya Interaction, Phys. Rev. Appl. **12**, 034005 (2019).

[24] T. Koyama, Y. Nakatani, J. Ieda, and D. Chiba, Electric field control of magnetic domain wall motion via modulation of the Dzyaloshinskii-Moriya interaction, Sci. Adv. **4**, eaav0265 (2018).

[25] See the Supplemental Material at http://link.aps.org/supplemental/10.1103/PhysRevApplied.14.064041 for details of the sample growth and characterization.

[26] A. Hubert and R. Schäfer, *Magnetic Domains, The Analysis of Magnetic Microstructures* (Springer, Berlin, 1998).

[27] B. Kaplan and G. A. Gehring, The domain structure in ultrathin magnetic films, J. Magn. Magn. Mater. **128**, 111 (1993).

[28] O. Boulle, J. Vogel, H. Yang, S. Pizzini, D. de Souza Chaves, A. Locatelli, T. O. Mentes, A. Sala, L. D. Buda-Prejbeanu, O. Klein, M. Belmeguenai, Y. Roussigné, Y. A. Stashkevich, S. M. Chérif, L. Aballe, M. Foerster, M. Chshiev, S. Auffret, I. M. Miron, and G. Gaudin, Room-temperature chiral magnetic skyrmions in ultrathin magnetic nanostructures, Nat. Nanotech. **11**, 449 (2016).

[29] R. Juge *et al.*, Current-Driven Skyrmion Dynamics and Drive-Dependent Skyrmion Hall Effect in an Ultrathin Film, Phys. Rev. Appl. **12**, 044007 (2019).

[30] A. Vansteenkiste, J. Leliaert, M. Dvornik, M. Helsen, F. Garcia-Sanchez, and B. Van Waeyenberge, The design and verification of MuMax3, AIP Adv. **4**, 107133 (2014).

[31] J. Mulkers, B. Van Waeyenberge, and M. V. Milosevic, Effects of spatially engineered Dzyaloshinskii-Moriya interaction in ferromagnetic films, Phys. Rev. B **95**, 144401 (2017).

[32] B. Barbara and M. Uehara, Magnetization processes in high anisotropy systems, Inst. Phys. Conf. Ser. 37, 204 (1978).

[33] J. Vogel, J. Moritz, and O. Fruchart, Nucleation of magnetisation reversal, from nanoparticles to bulk materials, C. R. Phys. **7**, 977 (2006).

[34] M. Labrune, S. Andrieu, F. Rio, and P. Bernstein, Time dependence of the magnetization process of Er-TM alloys, J. Magn. Magn. Mat. **80**, 211 (1989).

[35] J. Pommier, P. Meyer, P. Penissard, J. Ferré, P. Bruno, and D. Renard, Magnetization Reversal in Ultrathin Ferromagnetic Films with Perpendicular Anisotropy: Domain Observations, Phys. Rev. Lett. **65**, 2054 (1990).

[36] A. J. Tan, M. Huang, S. Sheffels, F. Büttner, S. Kim, A. H. Hunt, I. Waluyo, H. L. Tuller, and G. S. D. Beach, Hydration of gadolinium oxide (GdO_x) and its effect on voltage-induced Co oxidation in a Pt/Co/GdO_x/Au heterostructure, Phys. Rev. Mater. **3**, 064408 (2019).

[37] A. J. Tan, M. Huang, C. O. Avci, F. Büttner, M. Mann, W. Hu, C. Mazzoli, S. Wilkins, H. L. Tuller, and G. S. D. Beach, Magneto-ionic control of magnetism using a solid-state proton pump, Nat. Mater. **18**, 35 (2019).

[38] D. B. Strukov and R. S. Williams, Exponential ionic drift: Fast switching and low volatility of thin-film memristors, Appl. Phys. A **94**, 515 (2009).

[39] H. J. T. Ellingham, Reducibilty of oxides and sulphides in metallurgical processes, J. Soc. Chem. Ind. (London) **63**, 125 (1944).

[40] V. G. Subba Rao, S. Ramdas, P. N. Mehrotra, and C. N. R. Rao, Electrical transport in rare-earth oxides, J. Solid State Chem. **2**, 347 (1970).

[41] H. A. Miran, M. Altarawneh, Z. N. Jaf, B. Z. Dlugogorski, and Z.-T. Jiang, Structural, electronic and thermodynamic properties of bulk and surfaces of terbium dioxide (TbO_2), Mater. Res. Express **5**, 085901 (2018).

[42] E. Shoko, M. F. Smith, and R. H. McKenzie, Charge distribution and transport properties in reduced ceria phases: A review, J. Phys. Chem. Solids **72**, 1482 (2011).

[43] P. V. Fursikov, M. N. Abdusalyamova, and F. A. Makhmudov, Structural features and magnetic behavior of nanocrystalline powders of terbium oxide prepared by the thermal decomposition of terbium acetate in air, J. Alloys Compd. **657**, 163 (2016).

[44] N. Wu, W. Wang, Y. Wei, and T. Li, Studies on the effect of nano-sized MgO in magnesium-ion conducting gel polymer electrolyte for rechargeable magnesium batteries energies, Energies **10**, 1215 (2017).

[45] M. O. Davis, Transport phenomena in aluminium oxide. Nasa Technical Note NASA TN D-2765 (1965).

[46] D. de Souza Chaves, F. Ajejas, V. Křižáková, J. Vogel, and S. Pizzini, Oxidation dependence of the Dzyaloshinskii-Moriya interaction in Pt/Co/MO_x trilayers (M = Al or Gd), Phys. Rev. B **99**, 144404 (2019).